ARMY RESEARCH LABORATORY

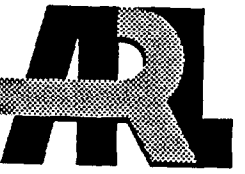

Ab Initio Potential Energy Surface for the H + OCS Reaction

Betsy M. Rice
Harry E. Cartland
Cary F. Chabalowski

ARL-TR-231

October 1993

NOTICES

Destroy this report when it is no longer needed. DO NOT return it to the originator.

Additional copies of this report may be obtained from the National Technical Information Service, U.S. Department of Commerce, 5285 Port Royal Road, Springfield, VA 22161.

The findings of this report are not to be construed as an official Department of the Army position, unless so designated by other authorized documents.

The use of trade names or manufacturers' names in this report does not constitute indorsement of any commercial product.

REPORT DOCUMENTATION PAGE

Form Approved
OMB No. 0704-0188

1. AGENCY USE ONLY (Leave blank)	2. REPORT DATE	3. REPORT TYPE AND DATES COVERED
	October 1993	Final, Feb 92 – Feb 93

4. TITLE AND SUBTITLE

Ab Initio Potential Energy Surface for the H + OCS Reaction

5. FUNDING NUMBERS

PR: 1L161102AH43

6. AUTHOR(S)

Betsy M. Rice, Harry E. Cartland, and Cary F. Chabalowski

7. PERFORMING ORGANIZATION NAME(S) AND ADDRESS(ES)

U.S. Army Research Laboratory
ATTN: AMSRL-WT-PC
Aberdeen Proving Ground, MD 21005-5066

8. PERFORMING ORGANIZATION REPORT NUMBER

9. SPONSORING / MONITORING AGENCY NAME(S) AND ADDRESS(ES)

U.S. Army Research Laboratory
ATTN: AMSRL-OP-CI-B (Tech Lib)
Aberdeen Proving Ground, MD 21005-5066

10. SPONSORING / MONITORING AGENCY REPORT NUMBER

ARL-TR-231

11. SUPPLEMENTARY NOTES

12a. DISTRIBUTION / AVAILABILITY STATEMENT

Approved for public release; distribution is unlimited.

12b. DISTRIBUTION CODE

13. ABSTRACT *(Maximum 200 words)*

An *ab initio* MP4 study has been made of the potential energy surface of the H + OCS reaction. Minima and saddle points leading to formation of OH + CS or SH + CO were found. Stationary points were located using the 6-31G** basis set at the ROHF and UMP2 levels of theory, with energy refinements at the MP4(SDTQ) level. Six minima corresponding to conformers of the HOCS system were calculated, and transition states leading into and out of these minima were determined. This theoretical study, in conjunction with the recent experimental results of Böhmer, Mikhaylichenko, and Wittig, provides a mechanistic overview of the reactions of the H + OCS system. The results substantiate earlier experimental hypotheses of the existence of stable, four-body reaction intermediates, as well as "tight" four-body transition states leading to products. Our results also show that these transition states have nonlinear structures, contrary to assumptions made in earlier experimental work. Our calculations provide the first set of structural data that detail the reaction mechanisms for H + OCS going to SH + CO or OH + CS. In addition, the features of this potential energy surface suggest explanations for observed nonstatistical behavior in product energy distributions of the SH + CO channel, and the statistical behavior observed in the product energy distributions of the OH + CS channel.

14. SUBJECT TERMS

potential energy surface, *ab initio*, MP4, electronic structure, potential energy, quantum chemistry

15. NUMBER OF PAGES

31

16. PRICE CODE

17. SECURITY CLASSIFICATION OF REPORT	18. SECURITY CLASSIFICATION OF THIS PAGE	19. SECURITY CLASSIFICATION OF ABSTRACT	20. LIMITATION OF ABSTRACT
UNCLASSIFIED	UNCLASSIFIED	UNCLASSIFIED	UL

INTENTIONALLY LEFT BLANK.

ACKNOWLEDGMENTS

The U.S. Army Research Office under the auspices of the U.S. Army Research Office Scientific Services Program administered by Battelle (Delivery Order 534, Contract No. DAAL03-91-C-0034) supported Harry E. Cartland during the preparation of this manuscript. The authors thank Böhmer, Mikhaylichenko, and Wittig for a preprint of their work, and Professors C. Wittig and B. Schlegel for helpful discussions.

INTENTIONALLY LEFT BLANK.

TABLE OF CONTENTS

INTENTIONALLY LEFT BLANK.

LIST OF FIGURES

LIST OF TABLES

INTENTIONALLY LEFT BLANK.

1. INTRODUCTION

Increasingly advanced experimental probing of molecular systems containing three or four atoms have contributed greatly to a detailed understanding of complex chemical behavior. Knowledge gleaned from these studies can be extrapolated to larger polyatomic systems to explain intricate chemical and physical processes which otherwise could not be unravelled due to the large number of reactions and degrees of freedom in bigger molecules.

Simple molecular systems are amenable to investigation through a variety of experimental and theoretical techniques. In experiments, chemical processes can be observed and resolved because complications arising from the number of secondary reactions and products are limited. From a theoretical standpoint, more sophisticated methods, which might be impossible to apply to a larger polyatomic, can be used to treat systems with small numbers of electrons. We present an *ab initio* MP4 study of the potential energy surface (PES) of such a small system, the hydrogen atom reaction with OCS.

There are two distinct reaction channels for this system that are expected to show dramatically different dynamic behavior because of a large difference in reaction enthalpy. The two reaction channels are:

$$H(^2S) + OCS(^1\Sigma) \text{ ---> } OH(^2\Pi) + CS(^1\Sigma) \qquad \Delta H^0298 = 57.2 \text{ kcal/mol} \qquad \text{(I)}$$

$$H(^2S) + OCS(^1\Sigma) \text{ ---> } SH(^2\Pi) + CO(^1\Sigma) \qquad \Delta H^0298 = -12.1 \text{ kcal/mol} \; . \qquad \text{(II)}$$

The earliest experimental studies of H + OCS concentrated on the kinetics of the sulphur abstraction reaction (II) (Tsunashima et al. 1975; Lee, Stief, and Timmons 1977). Absolute rate parameters for (II) were given in separate studies (Tsunashima et al. 1975; Lee, Stief, and Timmons 1977), but no mechanistic arguments were made. Reported activation energies (3.85 kcal/mol) were in good agreement, although the pre-exponential factors differed by a factor of 1.7. Both groups concluded that the small pre-exponential factor, when compared to other hydrogen abstraction reactions, suggests a low entropy of activation that can be explained by a tight activated complex.

The results of new state-selective experiments by Böhmer et al. (to be published) and Nickolaisen et al. (to be published), as well as earlier work by Häusler et al. (1987), have led to speculation about the mechanisms of (I) and (II). Häusler et al. (1987) measured SD and OD product internal energy

distributions in studies of deuterium scattering at high collision energy (60 kcal/mol). Experiments were performed under both bulk gas phase and precursor-geometry-limited (PGL or complexed) conditions, with 193-nm photolysis of DBr serving as the D atom source. These authors found that the SD distributions for (II) were colder than expected from statistical theory, while OD distributions for (I) were near statistical. Under bulk conditions, Nickolaisen et al. (to be published) studied reactive collisions of hot hydrogen atoms with OCS at energies up to 32 kcal/mol, which is lower than the threshold for formation of the products of (I). CO internal energy distributions were nonstatistically cold, with a particular bias against rotation. Most recently, Böhmer et al. (to be published) have reexamined OD and SD products from the D atom analogues of (I) and (II). SD and OD nascent distributions were again measured under bulk and complexed conditions, with DBr and DI as the hot atom sources. The SD distributions were essentially the same under bulk and complexed conditions, showed little dependence on collision energy (between 44 and 58 kcal/mol), and were consistently colder than statistical predictions. Partitioning in the OD product showed a similar lack of dependence on initial precursor orientation. All of these authors have suggested that formation of four-body intermediates might be important, but the details of the reaction mechanisms have been the subject of some debate.

The current theoretical study sheds light on the mechanistic details of (I) and (II), and provides crucial information to augment the recent state selective studies. Important mechanistic questions raised and addressed in this work are: (1) What are the primary reaction paths for (I) and (II)? (2) Does the hydrogen attack the OCS molecule end-on or broadside? (3) Do stable four-body intermediates exist? (4) Does hydrogen migration play a role in the reactions? (5) What are the characteristics of the activated complexes of the reactions? Besides addressing these questions, the details of the PES offer explanations for the experimentally observed product internal energy distributions of (I) and (II).

2. METHODS

Stationary points on the H + OCS ground state PES were located by restricted open-shell Hartree Fock (ROHF) calculations and by unrestricted Hartree Fock calculations with second-order Moller-Plesset correlation energy corrections (UMP2), both using the 6-31G** basis set (Francl et al. 1982). Harmonic vibrational frequencies were calculated for each stationary point on both ROHF and UMP2 surfaces, providing the zero point energy and characterization of each extremum. The ROHF optimized structures and subsequent fourth-order Moller-Plesset correlation energy corrections (ROMP4) were calculated using Version 5.0 of the CADPAC series of quantum chemistry codes (Amos and Rice 1992). The UMP2

optimized structures, and subsequent projected MP4 corrections (PUMP4), were calculated using the Gaussian 92 set of quantum chemistry codes (Frisch et al. 1992).

Many useful theoretical studies of molecular structures have been published in the last 10 years using theory at or below the level used here. We refer the interested reader to a few such studies for stable structures (Gould and Kollman 1992; Lammertsma et al. 1989), with favorable comparison to experimental data, when available (Simandiras et al. 1989; Brédas and Street 1988; and Ewing 1989), and others showing good qualitative agreement between MP theory and complete active space MCSCF (Koch et al. 1986, Tse 1990). In addition, similar informative studies published on energies and structures of transition states (Gould and Kollman 1992; Shi and Boyd 1990, 1991; Gordon and Truhlar 1986) show results consistent with experimental data when available (Tucker and Truhlar 1989; Sosa and Schlegel 1989, 1990). The MP2/6-31G** level of theory has been very successful in providing structural and mechanistic insight in these studies. UMP2 is known to be applicable to systems well represented by the UHF determinant (Simandiras et al. 1988). Using spin contamination as a metric (Table 1), all but one of the points show unprojected UHF S^2 values of 0.85 or less. (The *cis*- to *trans*-HOCS isomerization barrier [species t, Table 1] has an unprojected S^2 value of 0.90). This indicates that the UHF determinants are reasonable zeroth-order approximations to the wavefunctions.

Table 1 provides the total energies and zero point energies of the stationary points at the different levels of theory. Figure 1 illustrates the geometries and relevant parameters of each point. Species notation used in Table 1 and Figure 1 will be maintained throughout the remainder of this report. Tables 2 and 3 give the energies of the stationary points relative to H + OCS and harmonic vibrational frequencies, respectively. Figure 2 shows a relative energy schematic of stationary points on the H + OCS surface. The energy values used in this figure are PUMP4 energies calculated at the UMP2/6-31G** optimized structures with no further geometry refinement. ROHF/6-31G** and UMP2/6-31G** intrinsic reaction coordinate (IRC) (Gonzalez and Schlegel 1989, 1990) calculations for one exit channel reaction were done with the Gaussian 92 set of codes (Frisch et al. 1992).

3. RESULTS

3.1. H + OCS ---> SH + CO. Five minima (species d-h) corresponding to four-body conformers were determined from both ROHF and UMP2 geometry optimizations. At all levels of theory, the HCOS conformer is the most stable, followed by the *trans*- and *cis*-HSCO species, respectively. Although these

Table 1. Total Energies (Hartrees), Zero Point Energies (kcal/mol) and S^2 of Species on the H + OCS Potential Energy Surface

#	Species	ROHF/6-31G** // ROHF/6-31G**	ROMP4/6-31G** // ROHF/6-31G**	PUMP2/6-31G** // UMP2/6-31G**	PUMP4/6-31G** // UMP2/6-31G**	ZPE/ ROHF/ 6-31G**	ZPE/ UMP2/ 6-31G**	S^2 (UHF)
a.	H + OCS	-510.758854	-511.230920	-511.202615	-511.236521	6.2	5.8	—
b.	SH + CO	-510.802502	-511.250475	-511.212866	-511.254883	7.6	7.1	0.76
c.	OH + CS	-510.688794	-511.141152	-511.093549	-511.143956	7.9	7.4	0.76
d.	HCOS	-510.785568	-511.250505	-511.215581	-511.253751	12.7	11.8	0.76
e.	*trans*-HSCO	-510.774096	-511.248902	-511.214480	-511.253019	10.9	10.2	0.77
f.	*cis*-HSCO	-510.771899	-511.245053	-511.209975	-511.248662	10.8	10.0	0.76
g.	*trans*-HOCS	-510.753674	-511.228132	-511.193046	-511.230537	12.9	12.5	0.80
h.	*cis*-HOCS	-510.755379	-511.227033	-511.191889	-551.229316	12.9	12.2	0.79
i.	OH --- CS	—	—	-511.102997	-511.152608	—	9.0	0.76
j.	H + OCS --> HCOS	-510.717451	-511.210728	-511.179330	-511.215962	7.4	7.0	0.81
k.	H + OCS --> *trans*-HSCO	-510.728574	-511.207154	-511.173491	-511.211408	10.0	8.9	0.77
l.	H + OCS --> *cis*-HSCO	-510.715989	-511.213244	-511.181083	-511.217418	6.6	6.3	0.85
m.	H + OCS --> *trans*-HOCS	-510.718277	-511.192149	-511.156608	-511.193942	11.8	11.1	0.78
n.	H + OCS --> *cis*-HOCS	-510.687896	-511.190095	-511.154269	-511.190222	7.2	7.1	0.85
o.	HCOS --> *trans*-HSCO	-510.693037	-511.191894	-511.157588	-511.194947	8.2	7.9	0.79
p.	HCOS --> *trans*-HOCS	-510.670737	-511.171822	-511.134681	-511.172866	8.6	8.7	0.81
q.	*trans*-HSCO --> *cis*-HSCO	-510.760871	-511.235630	-511.202034	-511.241651	9.9	9.2	0.79
r.	*trans*-HSCO --> SH + CO	-510.767647	-511.245849	-511.208589	-511.249464	9.5	8.8	0.81
s.	*cis*-HSCO --> SH + CO	-510.762471	-511.240516	-511.204320	-511.245301	9.1	8.5	0.81
t.	*trans*-HOCS ---> *cis*-HOCS	-510.739085	-511.212070	-511.173436	-511.210546	11.8	11.3	0.90
u.	*trans*-HOCS --> OH --- CS	-510.663651	-511.160520	-511.099998	-511.149435	10.0	9.0	0.84

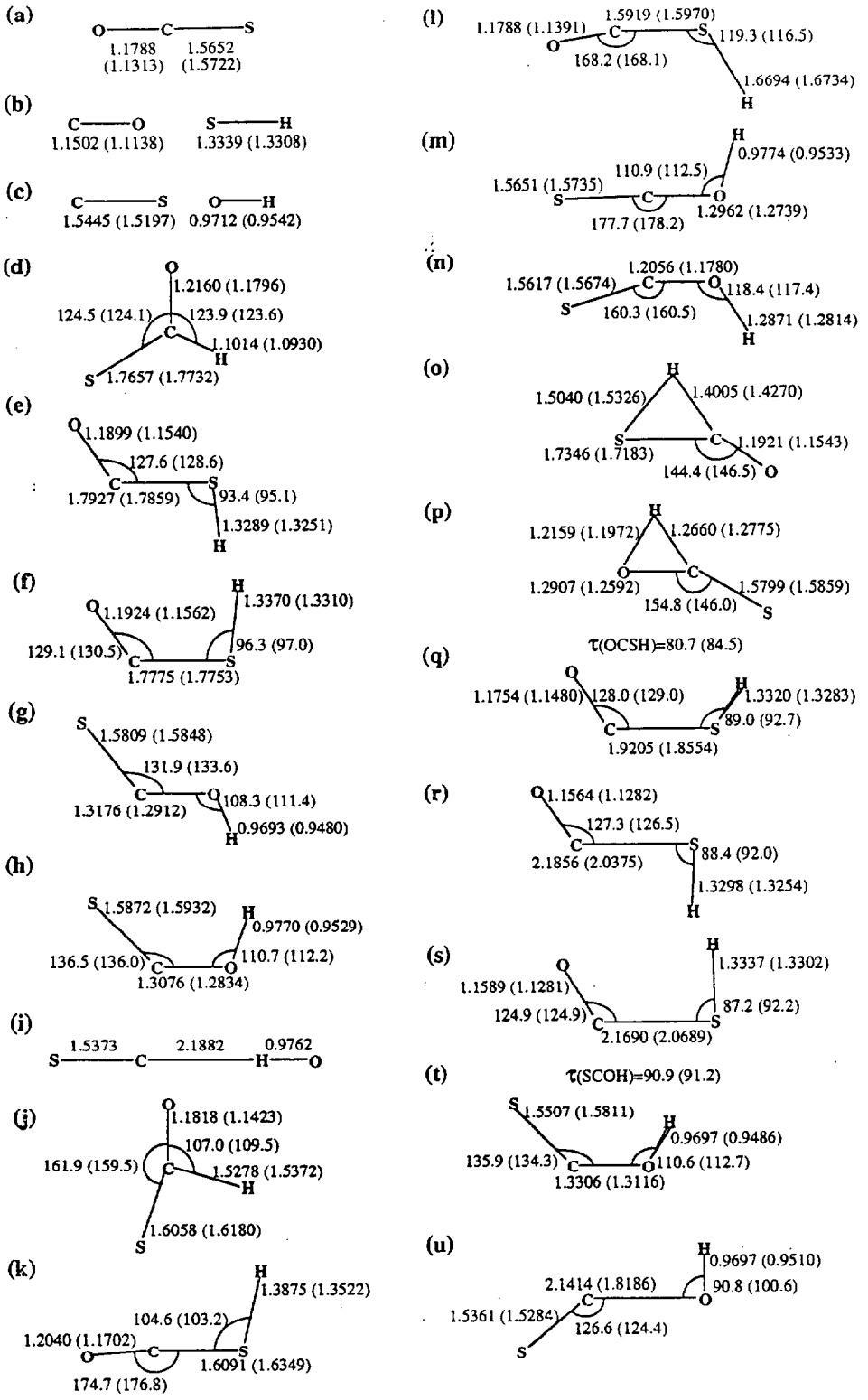

Figure 1. Optimized structures and geometric parameters at the UMP2/6-31G** level. The values of the geometric parameters of the optimized structure at the ROHF/6-31G** level are given in parentheses. Species (a)-(u) correspond to structures listed in Tables 1, 2, and 3.

Table 2. Relative Energy (kcal/mol) of Species on the H + OCS Potential Energy Surface

#	Species	ROHF/6-31G** //ROHF/6-31G**	ROMP4/6--31G** //ROHF/6-31G**	PUMP2/6-31G** //UMP2/6-31G**	PUMP4/6-31G** //UMP2/6-31G**
a.	H + OCS	0.0	0.0	0.0	0.0
b.	SH + CO	-27.4	-12.3	-6.4	-11.5
c.	OH + CS	44.0	56.3	68.4	58.1
d.	HCOS	-16.8	-12.3	-8.1	-10.8
e.	*trans*-HSCO	-9.6	-11.3	-7.4	-10.4
f.	*cis*-HSCO	-8.2	-8.9	-4.6	-7.6
g.	*trans*-HOCS	3.2	1.8	6.0	3.8
h.	*cis*-HOCS	2.2	2.4	6.7	4.5
i.	OH --- CS	—	—	62.5	52.7
j.	H+OCS --> HCOS	26.0	12.7	14.6	12.9
k.	H+OCS --> *trans*-HSCO	19.0	14.9	18.3	15.8
l.	H+OCS --> *cis*-HSCO	26.9	11.1	13.5	12.0
m.	H + OCS --> *trans*-HOCS	25.5	24.3	28.9	26.7
n.	H + OCS --> *cis*-HOCS	44.5	25.6	30.3	29.0
o.	HCOS --> *trans*-HSCO	41.3	24.5	28.3	26.1
p.	HCOS --> *trans*-HOCS	55.3	37.1	42.6	39.9
q.	*trans*-HSCO --> *cis*-HSCO	-1.3	-3.0	0.4	-3.2
r.	*trans*-HSCO --> SH + CO	-5.5	-9.4	-3.7	-8.1
s.	*cis*-HSCO --> SH + CO	-2.3	-6.0	-1.1	-5.5
t.	*trans*-HOCS --> *cis*-HOCS	12.4	11.8	18.3	16.3
u.	*trans*-HOCS --> OH --- CS	59.7	44.2	64.4	54.6

Table 3. Vibrational Frequencies (cm^{-1})

#	Species	ROHF/6-31G**	UMP2/6-31G**	EXPT.[a]
a.	H + OCS	567	503	520
		567	503	520
		890	902	859
		2,307	2,116	2,062
b.	SH	2,881	2,828	2,712
	CO	2,440	2,124	2,170
c.	OH	4,070	3,844	3,738
	CS	1,426	1,314	1,285
d.	HCOS	447	383	
		771	724	
		1,041	949	—
		1,496	1,413	
		1,976	1,759	
		3,162	3,040	
e.	*trans*-HSCO	395	388	
		430	399	
		681	632	—
		1,071	995	
		2,123	1,865	
		2,915	2,854	
f.	*cis*-HSCO	415	408	
		445	412	
		661	577	
		1,016	936	—
		2,119	1,859	
		2,867	2,781	
g.	*trans*-HOCS	488	460	
		532	606	
		980	1,023	—
		1,373	1,310	
		1,548	1,501	
		4,120	3,822	
h.	*cis*-HOCS	483	467	
		633	644	
		983	981	—
		1,372	1,279	
		1,533	1,518	
		4,032	3,671	

[a] Herzberg (1979); Huber and Herzberg (1979)

Table 3. Vibrational Frequencies (cm^{-1}) (continued)

#	Species	ROHF/6-31G**	UMP2/6-31G**	EXPT.[a]
i.	OH --- CS	—	52 59 136 457 463 1,345 3,748	—
j.	H+OCS --> HCOS	2,450*i* 605 643 785 929 2,194	1,489*i* 576 618 716 931 2,021	—
k.	H + OCS --> *trans*-HSCO	841*i* 477 735 1,010 2,198 2,599	756*i* 442 718 920 2,014 2,112	—
l.	H + OCS --> *cis*-HSCO	3,855*i* 436 536 558 873 2,246	1,531*i* 428 512 568 868 2,042	—
m.	H + OCS --> *trans*-HOCS	807*i* 438 794 1,341 1,709 3,980	801*i* 429 820 1,234 1,725 3,588	—
n.	H + OCS --> *cis*-HOCS	5,867*i* 436 638 921 997 2,020	3,327*i* 466 606 952 967 2,006	—

[a] Herzberg (1945); Huber and Herzberg (1979)

Table 3. Vibrational Frequencies (cm^{-1}) (continued)

#	Species	ROHF/6-31G**	UMP2/6-31G**	EXPT.[a]
o.	HCOS --> *trans*-HSCO	2,578*i* 415 512 773 1,890 2,113	1,918*i* 325 476 743 1,869 2,099	—
p.	HCOS --> *trans*-HOCS	2,807*i* 521 525 948 1,589 2,457	1,914*i* 527 531 996 1,572 2,445	—
q.	*trans*-HSCO --> *cis*-HSCO	3,841*i* 415 631 871 2,126 2,888	342*i* 306 541 770 1,975 2,830	—
r.	*trans*-HSCO --> SH + CO	689*i* 284 380 878 2,183 2,916	318*i* 215 307 739 2,047 2,852	—
s.	*cis*-HSCO --> SH + CO	782*i* 228 350 741 2,176 2,879	383*i* 150 307 641 2,016 2,821	—
t.	*trans*-HOCS --> *cis*-HOCS	678*i* 506 1,025 1,141 1,497 4,114	855*i* 507 965 1,113 1,483 3,837	—
u.	*trans*-HOCS --> OH ---CS	1,181*i* 276 285 936 1,358 4,116	321*i* 169 195 668 1,387 3,867	—

[a] Herzberg (1945); Huber and Herzberg (1979)

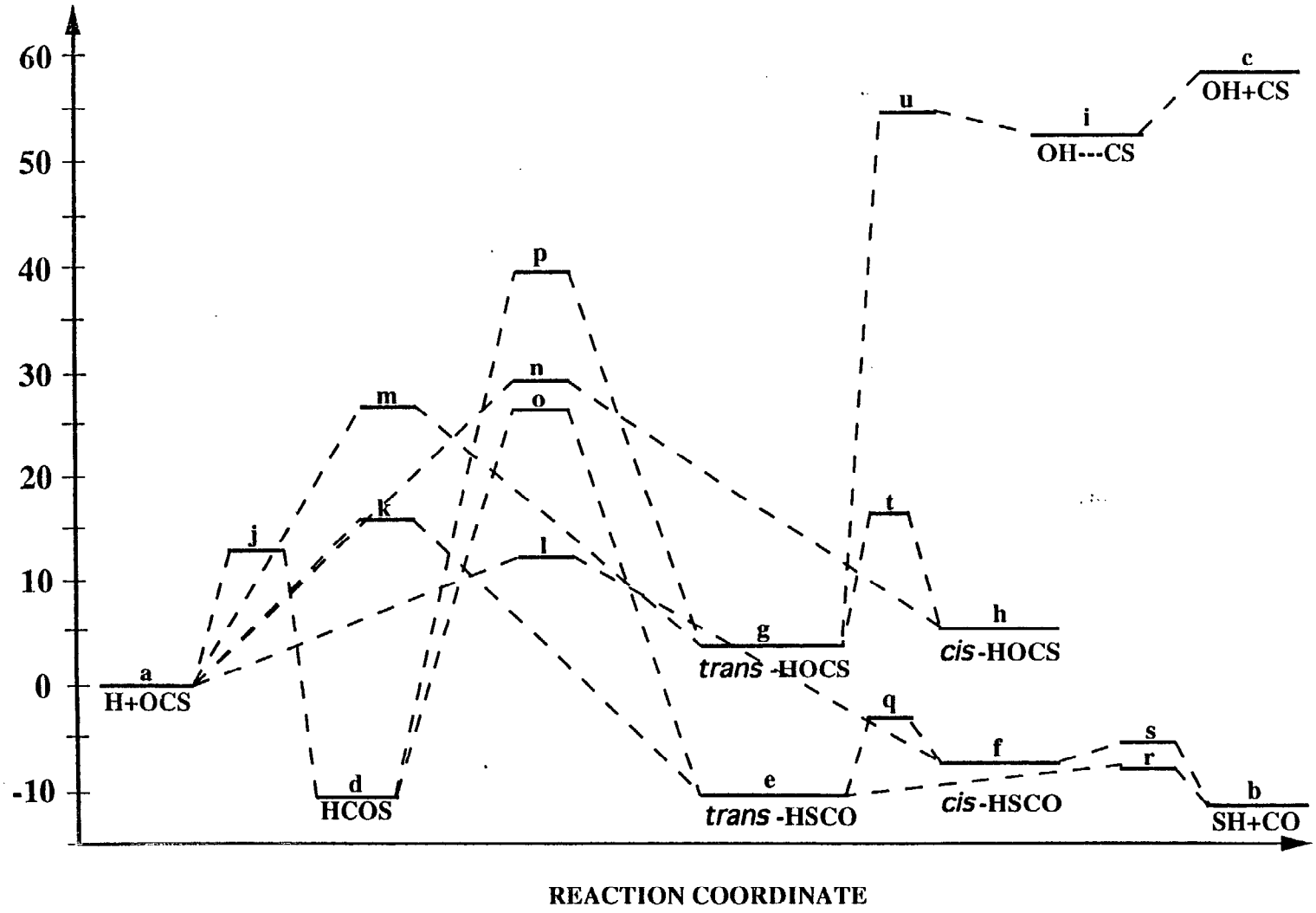

Figure 2. Energy level diagram for the H + OCS potential energy surface showing the minima and saddle point energies at the PUMP4//UMP2/6-31G** level.

complexes are lower in energy than H + OCS, the barriers to formation are substantial. The lowest entrance channel barrier among these three (transition states j-l) at the highest level of theory leads to formation of cis-HSCO (transition state l) and has a PUMP4 energy value of 12 kcal/mol. The energy barrier to formation of HCOS (transition state j) is the next higher at 13 kcal/mol. The barriers leading out of this minimum toward products (transition states o and p) are at least twice as large as the entrance channel barrier. This suggests that recrossing toward H + OCS is more likely to occur than isomerization to another four-body intermediate. The barriers to formation of SH + CO from the *trans*- and *cis*-HSCO minima (transition states r and s) are both approximately 2 kcal/mol. Based on energetics only, it seems most likely that formation of SH + CO will occur through direct formation of *cis*- or *trans*-HSCO by H atom attack on the S end of OCS.

3.2 H + OCS ---> OH + CS. The *cis*- and *trans*-HOCS minima are slightly higher in energy than separated H + OCS, and the entrance channel barriers are 29 and 27 kcal/mol, respectively. These are twice as large as those that lead to formation of the other stable intermediates. We were unable to find a transition state structure leading from the *cis*-HOCS well to OH + CS. The transition state (labeled u) leading from *trans*-HOCS has an energy that is almost as large as the enthalpy of (I).

Initially, we had assumed that transition state u led directly to OH + CS since its ROHF energy was higher than the energy of the products. However, the ROMP4, PUMP2, and PUMP4 transition state energies are all lower than that of the products, indicating that this assumption is incorrect. The ROHF/6-31G**, UHF/6-31G**, and UMP2/6-31G** IRCs leading from transition state u were calculated, and are shown in Figure 3(a). The energy of each point along the reaction coordinate is relative to the energy of the optimized transition state structure at each level of theory. The UMP2 and UHF IRC's stop upon reaching local minima at −5 and −10 kcal/mol relative to the transition state energy, respectively. The structure of the complex corresponding to this minimum is very nearly linear [Figure 1(i)]. The OHC and HCS angles are less than 0.01 from linearity, with the hydrogen end of the OH moiety oriented toward the carbon side of the CS portion of the molecule. The normal mode analysis for this structure indicates that it is stable (5 zero frequencies and no imaginary frequencies [Table 3]). There are two pairs of frequencies that are nearly degenerate (Table 3) as expected for a linear complex.

The geometry changes of the HOCS species as it moves from transition state u to the linear complex labelled (i) in Figure 1 is most apparent in the change of the COH angle as a function of reaction coordinate [shown in Figure 3(b)]. In the progression of the UMP2 and UHF IRC's from transition state

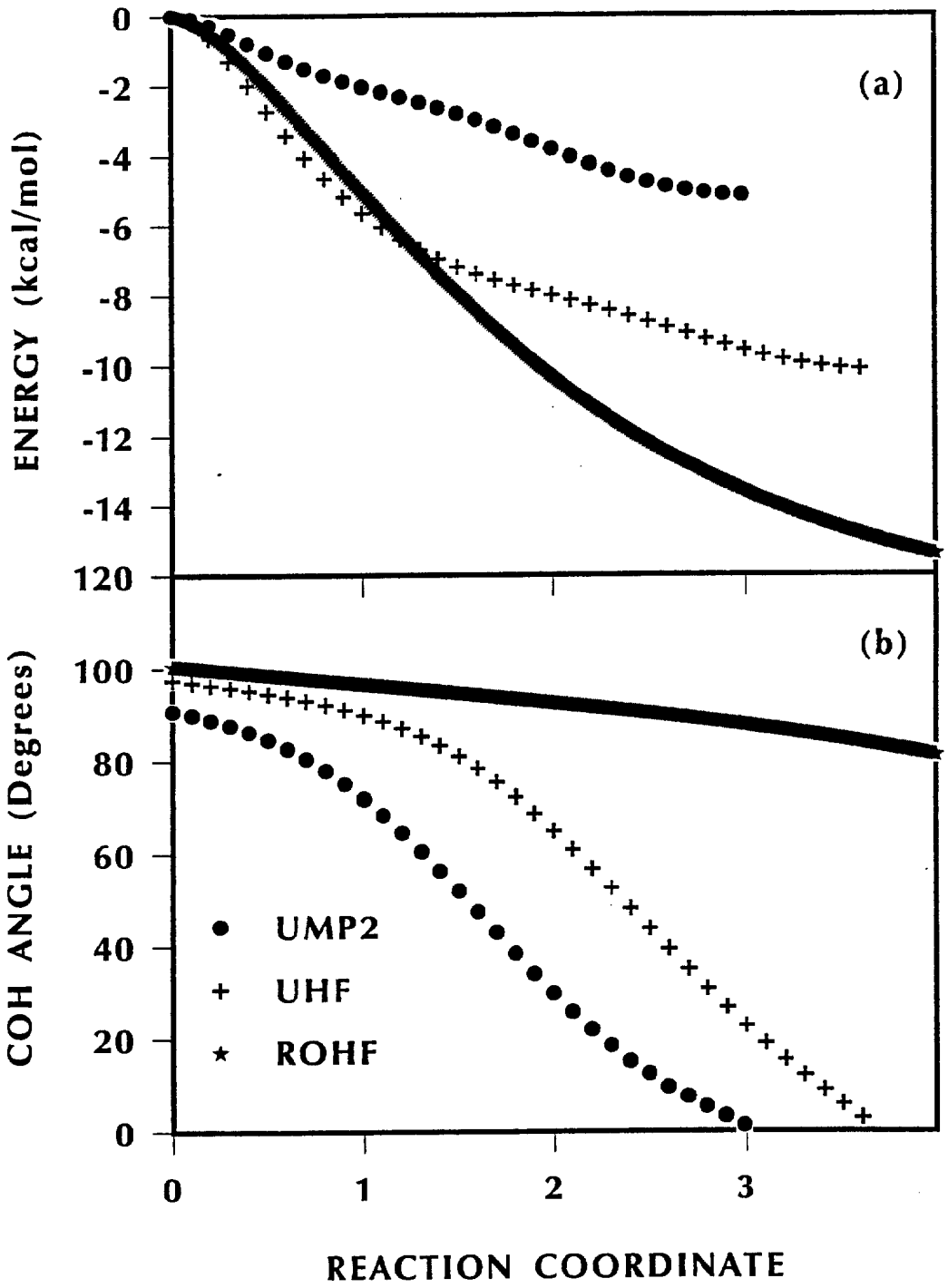

Figure 3. (a) Energies relative to energy of transition state u as a function of reaction coordinate at the UMP2, UHF, and ROHF levels of theory; (b) COH angle as a function of reaction coordinate. The IRC calculations lead from transition state u (see text).

u, the CO bond elongates and the COH bond angle decreases from 90° to 0°. This indicates that the O-H "flips" to form the linear structure shown in Figure 1(i). This reorientation was not observed in the ROHF IRC. The C-O bond lengthens but the COH angle changes little from its value at the transition state. The energy at the end of the ROHF IRC is −16 kcal/mol relative to the energy of the transition state, which is the same as the energy of the products.

Because this transition state [Figure 1(u)] led to different types of minima at the different levels of theory, we thought it useful to examine the normal mode corresponding to the imaginary frequency for this transition state at the two levels of theory (Figure 4). The geometry is similar at both ROHF and UMP2 levels of theory, and surprisingly, the eigenvectors corresponding to this mode are strikingly similar, giving no indication of the different minima to which these transition states lead. Also, very small steps had to be taken for the ROHF walk. This was due to convergence problems at this level of theory. The convergence problems at the ROHF level of theory, as well as the appearance in the UHF and UMP2 calculations of the slightly stable intermediate in the exit channel, suggest a low-lying excited electronic state in this spatial region. To investigate this further would be outside the scope of this study.

4. DISCUSSION

Temperature corrected MP4 enthalpies for T = 298 K of the asymptotic species have been calculated for comparison with experiment. For SH + CO, our best theoretical prediction of −10 kcal/mol is slightly higher than the experimental value of -12.1 ± 1.2 kcal/mol (Chase et al. 1985). For OH + CS, theory predicts 60 kcal/mol while the experimental value is 57.2 ± 6.0 kcal/mol (Chase 1985). Although the four-body species previously discussed have not been observed directly, experiments have provided criteria for them. It has been suggested that the activated complex for (II) is "tight" due to a low entropy of activation (i.e., small pre-exponential factor) (Tsunashima et al. 1975; Lee, Stief, and Timmons 1977). This proposal assumes a single linear activated complex, with degenerate HSC bending frequencies of 400 cm^{-1} (Tsunashima 1975). In our calculations, the pair of lowest vibrational frequencies for the saddle point complex between H + OCS and *cis*-HSCO are 428 and 512 cm^{-1}, respectively. Though the calculated complex is not linear, (as assumed in the experimental analyses), the calculated vibrational frequencies support the conclusion of a "tight" activated complex for (II).

At this level of theory, transition state energies are empirically observed to be overestimated (Gordon and Truhlar 1986; Tucker and Truhlar 1989; and Sosa and Schlegel 1987). In this study, the lowest

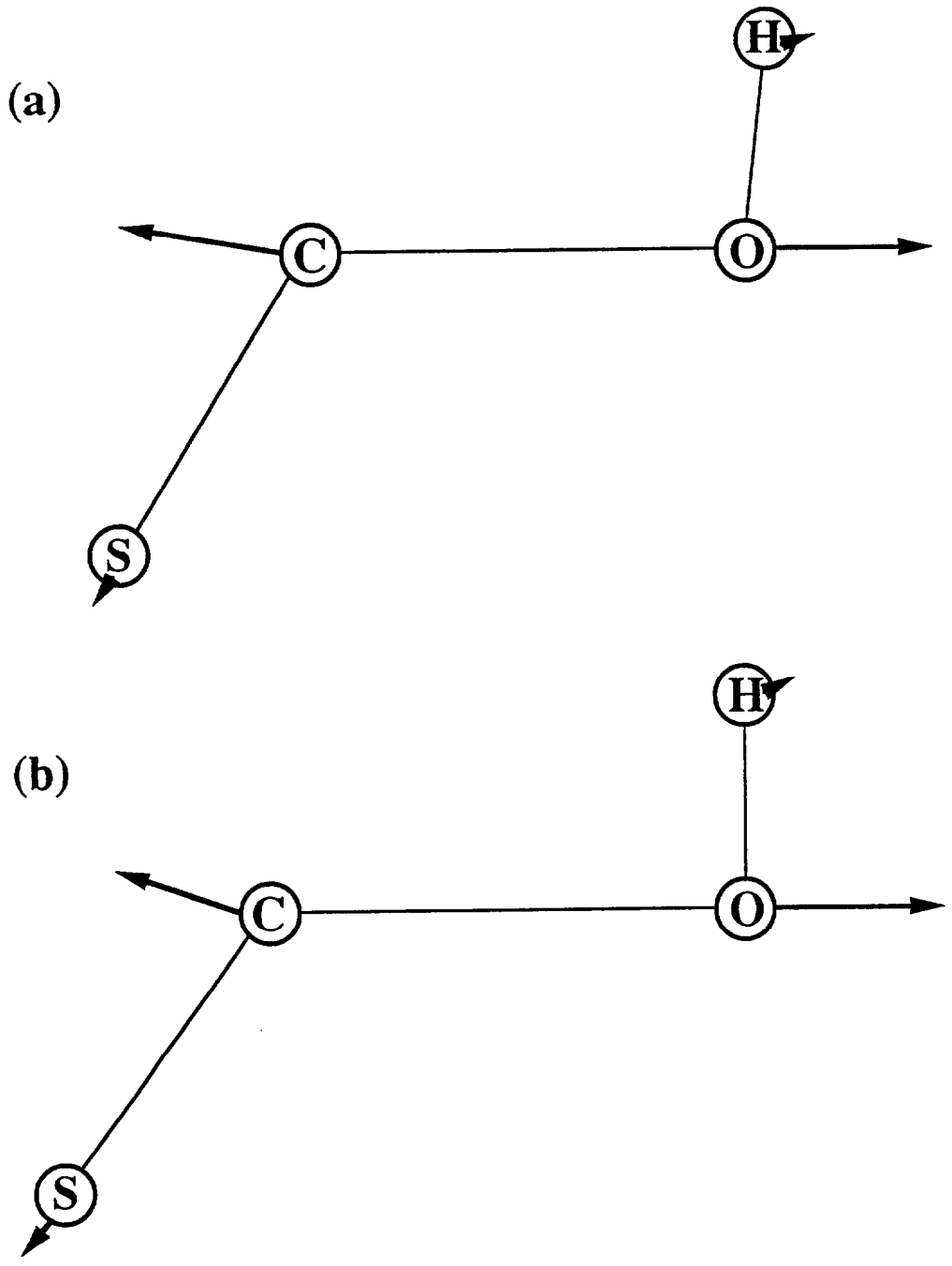

Figure 4. Depiction of the normal mode associated with the imaginary frequency at transition state (u) at the (a) ROHF/6-31G** level, (b) UMP2/6-31G** level.

energy entrance channel barrier calculated for (II) corresponds to formation of *cis*-HSCO (species f). The calculated entrance barrier to formation of *trans*-HSCO (species e) is 4 kcal/mol larger than the *cis*-HSCO barrier. If this energy separation is accurate, then most reactions would occur through formation of *cis*-HSCO, and the experimental activation energy for (II) should be associated with the *cis*- entrance channel barrier. Unfortunately, this level of theory is not sufficiently accurate to rule out the *trans*- barrier as a competing pathway, since 4 kcal/mol is probably within the uncertainty of these calculations. Due to the possibility of competing pathways and the uncertainties in the saddle point energies, the barrier height for formation of *cis*-HSCO cannot be directly associated with the experimental activation energy (3.85 kcal/mol). Quantitative comparisons must await the results of more accurate calculations and are outside the goals of this study.

Under gas phase, low-energy, single collision conditions, the SH and CO products most likely derive from direct S atom attack through side-on H atom approach trajectories (see Figures 1 and 2). As the collision energy increases, attack at the central carbon atom or the oxygen atom followed by H atom migration becomes feasible. At high energies, reactive approach geometries are less narrowly constrained since more of the PES is accessible. Changes in mechanism may be caused by other factors as well, so that in an extreme case, a "higher energy" channel might come to dominate the kinetics. Häuser, Rice, and Wittig (1987) and Böhmer, Mikhaylichenko, and Wittig (to be published) have both studied (II) under PGL conditions by complexing a D atom source with OCS. The structure of the DI-OCS van der Waals complex used in the latter study has not been resolved. However, recent high resolution spectroscopic measurements of the analogous HBr-OCS complex have revealed a quasi-linear structure with the H atom thought oriented toward the oxygen (Sharpe, private communication). Thus, it appears likely that photo-initiated SD production in DBr-OCS, and by analogy DI-OCS, involves D atom migration. It remains to be seen if there is a shift in the dominant mechanism due solely to limitations on the H atom approach, or if the presence of the halogen atom causes significant changes in the features of the PES.

The features on our calculated PES provide a qualitative explanation of the observed product state distributions. For (II), Nickolaisen and Cartland (to be published) determined that the SH product could have an internal energy of as much as 49% of that available. Häusler, Rice, and Wittig (1987) and Böhmer, Mikhaylichenko, and Wittig (to be published) observed that the SD rotational distributions were substantially colder than predicted by statistical theory. Nickolaisen et al. thus concluded that vibrational excitation must account for a large fraction of the total SH internal energy.

The features of the current PUMP4 PES can explain qualitatively the observed nonstatistical behavior. To illustrate, we will consider the formation of the products via the path with the lowest transition state energy only, the *cis*-HSCO complex. A simplistic one-dimensional reaction model through this path is shown in Figure 5. The reaction path for the formation of the products via the *trans*-HSCO complex is very similar to that of the *cis*-HSCO species. Therefore, for clarity, we will not include this path in our arguments.

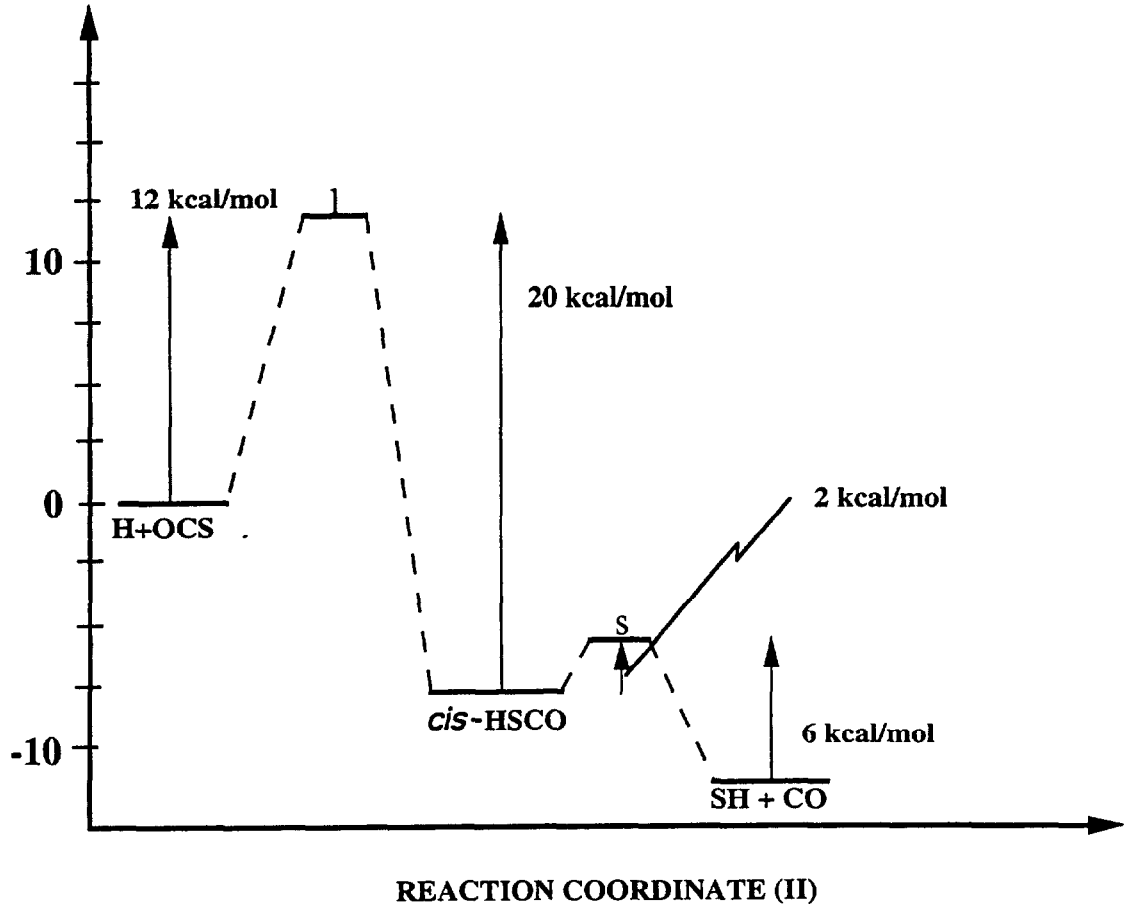

Figure 5. Energy diagram for the reaction channel leading to formation of SH + CO via the cis-HSCO minimum at the PUMP4//UMP2/6-31G** level. Energies along with the ordinate are in kcal/mol.

Upon formation of *cis*-HSCO, the molecule has at least 18 kcal/mol of energy in excess of that needed to go on to products. Most of the energy of the nascent *cis*-HSCO complex is stored in the newly formed S-H stretching and HSC bending modes. As intramolecular vibrational relaxation (IVR) begins, energy leaks out of the hot vibrations into the other modes of the complex, including the S-C stretch, which is

the reaction coordinate. The S-C stretch, however, requires only 2 kcal/mol to dissociate to products. Since this is only a small fraction of the available energy, the complex dissociates to SH+CO, leaving substantial energy in S-H vibration. Additional energy is released as the exit barrier is traversed and is partitioned among product degrees of freedom, according to the exit channel dynamics.

Our picture is one of a short-lived intermediate with large S-H vibrational excitation upon its formation, and incomplete IVR as the complex crosses to products. This mechanism is consistent with the experimental observations of Nickolaisen and Cartland (to be published), who found non-statistically cold CO and inferred vibrationally hot SH for (II). The overall features of the potential energy surface for this reaction path are qualitatively correct; if the magnitudes of the two barriers leading into and out of the *cis*-HSCO well were comparable in energy, more complete IVR would be expected. Additionally, if the exit channel barrier was higher relative to the final product energy, one might again expect to see hotter CO.

Converse arguments are consistent with the energy distributions observed by Häuser, Rice, and Wittig (1987) and Böhmer, Mikhaylichenko, and Wittig (to be published) for the deuterium analog of (I). These authors found nascent distributions that were statistical for OD, and suggested that this was due to a PES on which the energy of the DOCS intermediate was comparable to the energy of the hot D atom. Our surface shows that this is at least partially correct. The *cis*- and *trans*-HOCS minima are only slightly higher in energy than the H + OCS asymptote. In contrast, the entrance channel barriers to formation of these complexes are very large, and the exit channel barriers are even larger, approaching the endothermicity of the reaction. Figure 6 shows formation of OH + CS via the *trans*-HOCS complex. Proceeding as above, the O-H and HOC vibrations are highly excited upon HOCS formation. However, for reaction to go on to products, an amount of energy comparable to the reaction enthalpy must be coupled into the reaction coordinate, the C-O vibration. In this case, the collision complex either recrosses the entrance channel barrier back to reactants, or survives long enough to localize a large fraction of the available energy in the C-O reaction coordinate. For a longer-lived HOCS complex, IVR will be complete, or nearly so, and energy partitioning statistical, in agreement with experiment. These arguments break down for initial relative translational energies far in excess of the PES features, and product distributions become nonstatistical as previously described.

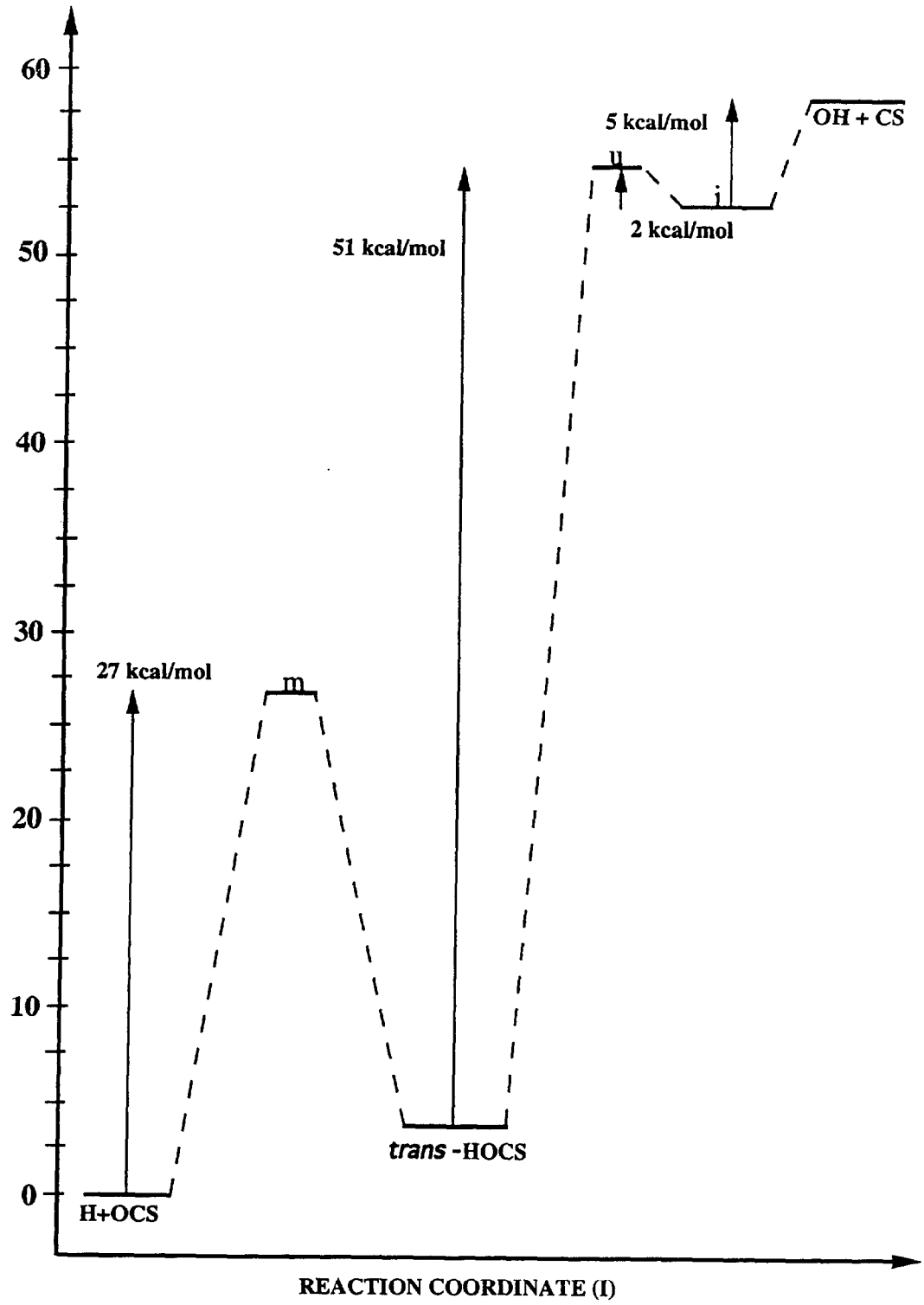

Figure 6. Energy level diagram for the reaction channel leading to formation of OH + CS via the trans-HOCS minimum at the PUMP4//UMP2/6-31G** level. Energies along the ordinate are in kcal/mol.

5. CONCLUSIONS

We have calculated minima and saddle points on the H + OCS ground state PES. Structures and energies were determined from geometry optimizations using a 6-31G** basis set at the ROHF and UMP2 levels of theory. Except for species (i), the geometric parameters of the optimized structures shown in Figure 1 differ very little between the two levels of theory. MP4 correlation corrections were calculated for each structure at both levels of theory, and the reaction enthalpies are in reasonable agreement with known experimental values. Six stable four-body intermediates were found. The hydrogen atom can be bound to either end of the OCS molecule in a nonlinear structure [species (e)-(h)], and to the carbon atom [species (d)]. In addition, a stable linear complex [species (i)] exists in which the hydrogen atom is inserted between the carbon and oxygen atoms.

The structures and high vibrational frequencies of the entrance channel transition states leading to formation of SH + CO support the conclusion that the activated complex for this reaction is "tight" (Tsunashima et al. 1975; Lee, Stief, and Timmons, 1977). Stable four-body *cis-* and *trans-* intermediates were found for both (I) and (II) in support of the experimental hypotheses put forth by Häusler, Rice and Wittig (1987), Nickolaisen and Cartland (to be published) and Böhmer, Mikhaylichenko, and Wittig (to be published). The structures of the entrance channel transition states show the four-body intermediates are reached by a broadside approach of the hydrogen atom, which is consistent with the explanation of Böhmer, Mikhaylichenko, and Wittig (to be published) based on orbital occupancy. Finally, the features of the surface offer explanations for both the non-statistical product energy distributions of SH + CO, and the statistical product energy distributions for OH + CS, observed in state-selective reactive scattering experiments of H and D with OCS.

INTENTIONALLY LEFT BLANK.

6. REFERENCES

Amos, R. D., and J. E. Rice. "CADPAC: The Cambridge Analytic Derivatives Package." Issue 5.0, Cambridge, 1992.

Böhmer, E., K. Mikhaylichenko and C. Wittig. J. Chem. Phys., submitted for publication.

Brédas, J. L., and G. B. Street. J. Am. Chem. Soc., vol. 110, p. 7001, 1988.

Chase, M. W., C. A. Davies, J. R. Downey, D. J. Frurip, R. A. McDonald, and A. N. Syverud. JANAF Thermochemical Tables, Third Edition. J. Phys. Chem., Ref. Data vol. 14, Supplement 1, 1985.

Ewing, D. W. J. Am. Chem. Soc., vol. 111, p. 8809, 1989.

Francl, M. M., W. J. Pietro, W. J. Hehre, J. S. Binkley, M. S. Gordon, D. J. DeFrees, and J. A. Pople. J. Chem. Phys., vol. 77, p. 3654, 1982.

Frisch, M. J., G. W. Trucks, M. Head-Gordon, F. M. W. Gill, M. W. Wong, J. B. Foresman, B. G. Johnson, H. B. Schlegel, M. A. Robb, E. S. Replogle, R. Gomperts, J. L. Andres, K. Raghavachari, J. S. Binkley, C. Gonzalez, R. L. Martin, D. J. Fox, D. J. Defrees, J. Baker, J. J. P. Stewart and J. A. Pople. *Gaussian 92*, Revision A. Gaussian, Inc., Pittsburgh, PA, 1992.

Gonzalez, C., and H. B. Schlegel. J. Phys. Chem., vol. 90, p. 2154, 1989.

Gonzalez, C., and H. B. Schlegel. J. Phys. Chem., vol. 94, p. 5523, 1990.

Gordon, M. S., and D. G. Truhlar. J. Am. Chem. Soc., vol. 108, p. 5412, 1986.

Gould, I. R., and P. A. Kollman. J. Phys. Chem., vol. 96, p. 9255, 1992.

Häusler, D., J. Rice and C. Wittig. J. Phys. Chem., vol. 91, p. 5413, 1987.

Koch, W., G. Frenking, J. Gauss, D. Cremer, A. Sawaryn, and P. V. Schleyer. J. Am. Chem. Soc., vol. 108, p. 5732, 1986.

Lammertsma, K., O. F. Güner, A. F. Thibodeaux, and P. V. Schleyer. J. Am. Chem. Soc., vol. 111, p. 8995, 1989.

Lee, J. H., L. J. Stief, and R. B. Timmons. J. Chem. Phys., vol. 67, p. 1705, 1977.

Nickolaisen, S. L., and H. E. Cartland. J. Chem. Phys., in press.

Sharpe, S. Pacific Northwest Laboratories, private communication.

Shi, Z., and R. Boyd. J. Am. Chem. Soc., vol. 112, p. 6789, 1990.

Shi, Z., and R. J. Boyd. J. Am. Chem. Soc., vol. 113, p. 2434, 1991.

Simandiras, E. D., R. D. Amos, N. C. Handy, T. J. Lee, J. E. Rice, R. B. Remington, and H. F. Schaefer. J. Am. Chem. Soc., vol. 110, p. 1388, 1988.

Sosa, C., and H. B. Schlegel. J. Am. Chem. Soc., vol. 109, p. 4193, 1987.

Tse, J. S. J. Am. Chem. Soc., vol. 112, p. 5060, 1990.

Tsunashima, S., T. Yokota, I. Safarik, H. E. Gunning, and O. P. Strausz. J. Phys. Chem., vol. 79, p. 775, 1975.

Tucker, S. C., and D. G. Truhlar. J. Phys. Chem., vol. 93, p. 8138, 1989.

No. of Copies	Organization
2	Administrator Defense Technical Info Center ATTN: DTIC-DDA Cameron Station Alexandria, VA 22304-6145
1	Commander U.S. Army Materiel Command ATTN: AMCAM 5001 Eisenhower Ave. Alexandria, VA 22333-0001
1	Director U.S. Army Research Laboratory ATTN: AMSRL-OP-CI-AD, Tech Publishing 2800 Powder Mill Rd. Adelphi, MD 20783-1145
1	Director U.S. Army Research Laboratory ATTN: AMSRL-OP-CI-AD, Records Management 2800 Powder Mill Rd. Adelphi, MD 20783-1145
2	Commander U.S. Army Armament Research, Development, and Engineering Center ATTN: SMCAR-IMI-I Picatinny Arsenal, NJ 07806-5000
2	Commander U.S. Army Armament Research, Development, and Engineering Center ATTN: SMCAR-TDC Picatinny Arsenal, NJ 07806-5000
1	Director Benet Weapons Laboratory U.S. Army Armament Research, Development, and Engineering Center ATTN: SMCAR-CCB-TL Watervliet, NY 12189-4050
1	Director U.S. Army Advanced Systems Research and Analysis Office (ATCOM) ATTN: AMSAT-R-NR, M/S 219-1 Ames Research Center Moffett Field, CA 94035-1000

No. of Copies	Organization
1	Commander U.S. Army Missile Command ATTN: AMSMI-RD-CS-R (DOC) Redstone Arsenal, AL 35898-5010
1	Commander U.S. Army Tank-Automotive Command ATTN: AMSTA-JSK (Armor Eng. Br.) Warren, MI 48397-5000
1	Director U.S. Army TRADOC Analysis Command ATTN: ATRC-WSR White Sands Missile Range, NM 88002-5502
(Class. only) 1	Commandant U.S. Army Infantry School ATTN: ATSH-CD (Security Mgr.) Fort Benning, GA 31905-5660
(Unclass. only) 1	Commandant U.S. Army Infantry School ATTN: ATSH-WCB-O Fort Benning, GA 31905-5000
1	WL/MNOI Eglin AFB, FL 32542-5000
	Aberdeen Proving Ground
2	Dir, USAMSAA ATTN: AMXSY-D AMXSY-MP, H. Cohen
1	Cdr, USATECOM ATTN: AMSTE-TC
1	Dir, ERDEC ATTN: SCBRD-RT
1	Cdr, CBDA ATTN: AMSCB-CII
1	Dir, USARL ATTN: AMSRL-SL-I
10	Dir, USARL ATTN: AMSRL-OP-CI-B (Tech Lib)

No. of Copies	Organization
1	HQDA, OASA (RDA) ATTN: Dr. C.H. Church Pentagon, Room 3E486 WASH DC 20310-0103
4	Commander US Army Research Office ATTN: R. Ghirardelli D. Mann R. Singleton R. Shaw P.O. Box 12211 Research Triangle Park, NC 27709-2211
2	Commander US Army Armament Research, Development, and Engineering Center ATTN: SMCAR-AEE-B, D.S. Downs SMCAR-AEE, J.A. Lannon Picatinny Arsenal, NJ 07806-5000
1	Commander US Army Armament Research, Development, and Engineering Center ATTN: SMCAR-AEE-BR, L. Harris Picatinny Arsenal, NJ 07806-5000
2	Commander US Army Missile Command ATTN: AMSMI-RD-PR-E, A.R. Maykut AMSMI-RD-PR-P, R. Betts Redstone Arsenal, AL 35898-5249
1	Office of Naval Research Department of the Navy ATTN: R.S. Miller, Code 432 800 N. Quincy Street Arlington, VA 22217
1	Commander Naval Air Systems Command ATTN: J. Ramnarace, AIR-54111C Washington, DC 20360
2	Commander Naval Surface Warfare Center ATTN: R. Bernecker, R-13 G.B. Wilmot, R-16 Silver Spring, MD 20903-5000

No. of Copies	Organization
5	Commander Naval Research Laboratory ATTN: M.C. Lin J. McDonald E. Oran J. Shnur R.J. Doyle, Code 6110 Washington, DC 20375
2	Commander Naval Weapons Center ATTN: T. Boggs, Code 388 T. Parr, Code 3895 China Lake, CA 93555-6001
1	Superintendent Naval Postgraduate School Dept. of Aeronautics ATTN: D.W. Netzer Monterey, CA 93940
3	AL/LSCF ATTN: R. Corley R. Geisler J. Levine Edwards AFB, CA 93523-5000
1	AFOSR ATTN: J.M. Tishkoff Bolling Air Force Base Washington, DC 20332
1	OSD/SDIO/IST ATTN: L. Caveny Pentagon Washington, DC 20301-7100
1	Commandant USAFAS ATTN: ATSF-TSM-CN Fort Sill, OK 73503-5600
1	University of Dayton Research Institute ATTN: D. Campbell AL/PAP Edwards AFB, CA 93523
1	NASA Langley Research Center Langley Station ATTN: G.B. Northam/MS 168 Hampton, VA 23365

No. of Copies	Organization
4	National Bureau of Standards ATTN: J. Hastie M. Jacox T. Kashiwagi H. Semerjian US Department of Commerce Washington, DC 20234
1	Applied Combustion Technology, Inc. ATTN: A.M. Varney P.O. Box 607885 Orlando, FL 32860
2	Applied Mechanics Reviews The American Society of Mechanical Engineers ATTN: R.E. White A.B. Wenzel 345 E. 47th Street New York, NY 10017
1	Atlantic Research Corp. ATTN: R.H.W. Waesche 7511 Wellington Road Gainesville, VA 22065
1	Textron Defense Systems ATTN: A. Patrick 2385 Revere Beach Parkway Everett, MA 02149-5900
1	Battelle ATTN: TACTEC Library, J. Huggins 505 King Avenue Columbus, OH 43201-2693
1	Cohen Professional Services ATTN: N.S. Cohen 141 Channing Street Redlands, CA 92373
1	Exxon Research & Eng. Co. ATTN: A. Dean Route 22E Annandale, NJ 08801
1	General Applied Science Laboratories, Inc. 77 Raynor Avenue Ronkonkama, NY 11779-6649

No. of Copies	Organization
1	General Electric Ordnance Systems ATTN: J. Mandzy 100 Plastics Avenue Pittsfield, MA 01203
1	General Motors Rsch Labs Physical Chemistry Department ATTN: T. Sloane Warren, MI 48090-9055
2	Hercules, Inc. Allegheny Ballistics Lab. ATTN: W.B. Walkup E.A. Yount P.O. Box 210 Rocket Center, WV 26726
1	Alliant Techsystems, Inc. Marine Systems Group ATTN: D.E. Broden/MS MN50-2000 600 2nd Street NE Hopkins, MN 55343
1	Alliant Techsystems, Inc. ATTN: R.E. Tompkins 7225 Northland Drive Brooklyn Park, MN 55428
1	IBM Corporation ATTN: A.C. Tam Research Division 5600 Cottle Road San Jose, CA 95193
1	IIT Research Institute ATTN: R.F. Remaly 10 West 35th Street Chicago, IL 60616
2	Director Lawrence Livermore National Laboratory ATTN: C. Westbrook W. Tao, MS L-282 P.O. Box 808 Livermore, CA 94550
1	Lockheed Missiles & Space Co. ATTN: George Lo 3251 Hanover Street Dept. 52-35/B204/2 Palo Alto, CA 94304

No. of Copies	Organization
1	Director Los Alamos National Lab ATTN: B. Nichols, T7, MS-B284 P.O. Box 1663 Los Alamos, NM 87545
1	National Science Foundation ATTN: A.B. Harvey Washington, DC 20550
1	Olin Ordnance ATTN: V. McDonald, Library P.O. Box 222 St. Marks, FL 32355-0222
1	Paul Gough Associates, Inc. ATTN: P.S. Gough 1048 South Street Portsmouth, NH 03801-5423
2	Princeton Combustion Research Laboratories, Inc. ATTN: N.A. Messina M. Summerfield Princeton Corporate Plaza Bldg. IV, Suite 119 11 Deerpark Drive Monmouth Junction, NJ 08852
1	Hughes Aircraft Company ATTN: T.E. Ward 8433 Fallbrook Avenue Canoga Park, CA 91303
1	Rockwell International Corp. Rocketdyne Division ATTN: J.E. Flanagan/HB02 6633 Canoga Avenue Canoga Park, CA 91304
3	Director Sandia National Laboratories Division 8354 ATTN: S. Johnston P. Mattern D. Stephenson Livermore, CA 94550
1	Science Applications, Inc. ATTN: R.B. Edelman 23146 Cumorah Crest Woodland Hills, CA 91364

No. of Copies	Organization
3	SRI International ATTN: G. Smith D. Crosley D. Golden 333 Ravenswood Avenue Menlo Park, CA 94025
1	Stevens Institute of Tech. Davidson Laboratory ATTN: R. McAlevy, III Hoboken, NJ 07030
1	Sverdrup Technology, Inc. LERC Group ATTN: R.J. Locke, MS SVR-2 2001 Aerospace Parkway Brook Park, OH 44142
1	Sverdrup Technology, Inc. ATTN: J. Deur 2001 Aerospace Parkway Brook Park, OH 44142
3	Thiokol Corporation Elkton Division ATTN: R. Biddle R. Willer Tech Lib P.O. Box 241 Elkton, MD 21921
3	Thiokol Corporation Wasatch Division ATTN: S.J. Bennett P.O. Box 524 Brigham City, UT 84302
1	United Technologies Research Center ATTN: A.C. Eckbreth East Hartford, CT 06108
1	United Technologies Corp. Chemical Systems Division ATTN: R.R. Miller P.O. Box 49028 San Jose, CA 95161-9028
1	Universal Propulsion Company ATTN: H.J. McSpadden 25401 North Central Avenue Phoenix, AZ 85027-7837

No. of Copies	Organization
1	Veritay Technology, Inc. ATTN: E.B. Fisher 4845 Millersport Highway P.O. Box 305 East Amherst, NY 14051-0305
1	Brigham Young University Dept. of Chemical Engineering ATTN: M.W. Beckstead Provo, UT 84058
1	California Institute of Tech. Jet Propulsion Laboratory ATTN: L. Strand/MS 125-224 4800 Oak Grove Drive Pasadena, CA 91109
1	California Institute of Technology ATTN: F.E.C. Culick/MC 301-46 204 Karman Lab. Pasadena, CA 91125
1	University of California Los Alamos Scientific Lab. P.O. Box 1663, Mail Stop B216 Los Alamos, NM 87545
1	University of California, Berkeley Chemistry Deparment ATTN: C. Bradley Moore 211 Lewis Hall Berkeley, CA 94720
1	University of California, San Diego ATTN: F.A. Williams AMES, B010 La Jolla, CA 92093
2	University of California, Santa Barbara Quantum Institute ATTN: K. Schofield M. Steinberg Santa Barbara, CA 93106
1	University of Colorado at Boulder Engineering Center ATTN: J. Daily Campus Box 427 Boulder, CO 80309-0427
3	University of Southern California Dept. of Chemistry ATTN: R. Beaudet S. Benson C. Wittig Los Angeles, CA 90007
1	Cornell University Department of Chemistry ATTN: T.A. Cool Baker Laboratory Ithaca, NY 14853
1	University of Delaware ATTN: T. Brill Chemistry Department Newark, DE 19711
1	University of Florida Dept. of Chemistry ATTN: J. Winefordner Gainesville, FL 32611
3	Georgia Institute of Technology School of Aerospace Engineering ATTN: E. Price W.C. Strahle B.T. Zinn Atlanta, GA 30332
1	University of Illinois Dept. of Mech. Eng. ATTN: H. Krier 144MEB, 1206 W. Green St. Urbana, IL 61801
1	The Johns Hopkins University Chemical Propulsion Information Agency ATTN: T.W. Christian 10630 Little Patuxent Parkway, Suite 202 Columbia, MD 21044-3200
1	University of Michigan Gas Dynamics Lab Aerospace Engineering Bldg. ATTN: G.M. Faeth Ann Arbor, MI 48109-2140
1	University of Minnesota Dept. of Mechanical Engineering ATTN: E. Fletcher Minneapolis, MN 55455

No. of Copies	Organization
3	Pennsylvania State University Applied Research Laboratory ATTN: K.K. Kuo H. Palmer M. Micci University Park, PA 16802
1	Pennsylvania State University Dept. of Mechanical Engineering ATTN: V. Yang University Park, PA 16802
1	Polytechnic Institute of NY Graduate Center ATTN: S. Lederman Route 110 Farmingdale, NY 11735
2	Princeton University Forrestal Campus Library ATTN: K. Brezinsky I. Glassman P.O. Box 710 Princeton, NJ 08540
1	Purdue University School of Aeronautics and Astronautics ATTN: J.R. Osborn Grissom Hall West Lafayette, IN 47906
1	Purdue University Department of Chemistry ATTN: E. Grant West Lafayette, IN 47906
2	Purdue University School of Mechanical Engineering ATTN: N.M. Laurendeau S.N.B. Murthy TSPC Chaffee Hall West Lafayette, IN 47906
1	Rensselaer Polytechnic Inst. Dept. of Chemical Engineering ATTN: A. Fontijn Troy, NY 12181
1	Stanford University Dept. of Mechanical Engineering ATTN: R. Hanson Stanford, CA 94305

No. of Copies	Organization
1	University of Texas Dept. of Chemistry ATTN: W. Gardiner Austin, TX 78712
1	Virginia Polytechnic Institute and State University ATTN: J.A. Schetz Blacksburg, VA 24061
1	Freedman Associates ATTN: E. Freedman 2411 Diana Road Baltimore, MD 21209-1525
1	Director Army Research Office ATTN: AMXRO-MCS, K. Clark P.O. Box 12211 Research Triangle Park, NC 27709-2211
1	Director Army Research Office ATTN: AMXRO-RT-IP, Library Services P.O. Box 12211 Research Triangle Park, NC 27709-2211